Quaternary Science Advances 15 (2024) 100208

Contents lists available at ScienceDirect

Quaternary Science Advances

journal homepage: www.sciencedirect.com/journal/quaternary-science-advances

Combining orbital tuning and direct dating approaches to age-depth model development for Chew Bahir, Ethiopia

Martin H. Trauth [a,*], Asfawossen Asrat [b,c], Markus L. Fischer [a], Verena Foerster [d], Stefanie Kaboth-Bahr [e], Henry F. Lamb [f,g], Norbert Marwan [h], Helen M. Roberts [f], Frank Schaebitz [d]

[a] University of Potsdam, Institute of Geosciences, Potsdam, Germany
[b] Botswana International University of Science and Technology, School of Earth Sciences and Engineering Palapye, Botswana
[c] Addis Ababa University, School of Earth Sciences, Addis Ababa, Ethiopia
[d] University of Cologne, Institute of Geography Education, Cologne, Germany
[e] Free University Berlin, Institute of Geological Sciences, Berlin, Germany
[f] Aberystwyth University, Department of Geography and Earth Sciences, Aberystwyth, UK
[g] Trinity College Dublin, Botany Department, School of Natural Sciences, Ireland
[h] Potsdam Institute for Climate Impact Research, Potsdam, Germany

A B S T R A C T

The directly dated *RRMarch2021* age model (Roberts et al., 2021) for the ~293 m long composite core from Chew Bahir, southern Ethiopia, has provided a valuable chronology for long-term climate changes in northeastern Africa. However, the age model has limitations on shorter time scales (less than 1–2 precession cycles), especially in the time range <20 kyr BP (kiloyears before present or thousand years before 1950) and between ~155 and 428 kyr BP. To address those constraints we developed a partially orbitally tuned age model. A comparison with the ODP Site 967 record of the wetness index from the eastern Mediterranean, 3300 km away but connected to the Ethiopian plateau via the River Nile, suggests that the partially orbitally tuned age model offers some advantages compared to the exclusively directly dated age model, with the limitation of the reduced significance of (cross) spectral analysis results of tuned age models in cause-effect studies. The availability of this more detailed age model is a prerequisite for further detailed spatiotemporal correlations of climate variability and its potential impact on the exchange of different populations of *Homo sapiens* in the region.

1. Introduction

The Chew Bahir Drilling Project (CBDP), initiated in November 2008, was part of the Hominin Sites and Paleolakes Drilling Project (HSPDP), aiming to provide continuous, high-resolution records of environmental change which span critical intervals of human evolution, dispersion, and cultural innovation (Cohen et al., 2016, 2022; Foerster et al., 2012, 2022; Schaebitz et al., 2021; Trauth et al., 2024; Fischer et al., 2024). In 2009 and 2010, we recovered several short cores CB01–06 along a ~20 km long NW–SE transect across the southern part of the basin, up to 18.8 m long and spanning the last ~47 kyrs (Foerster et al., 2012, 2015; Trauth et al., 2018) (Table 1, Fig. 1). In May 2014, a ~40 m long core CHB14-1 was collected from the central part of the southern Chew Bahir basin covering the last ~120 kyrs (Viehberg et al., 2018). During a 35-day coring campaign in Nov–Dec 2014, two ~280 m long parallel cores CHB14-2A and 2B were collected that were subsequently merged to a ~293 m long composite core CHB14-2 (Foerster et al., 2022). The age models of the short cores CB01–06 and the intermediate core CHB14-1 that cover the younger sedimentary deposits were discussed in separate publications (e.g., Foerster et al., 2012, 2015; Viehberg et al., 2018; Trauth et al., 2018, 2019, 2024). The age model of CHB14-2 named RRMarch2021 followed a direct-dating approach and was presented in Roberts et al. (2021) providing a reliable first chronology for the Chew Bahir composite core spanning the last ~620 kyrs. The RRMarch2021 age model has been used in several studies related to different topical foci in paleoclimate dynamics reconstructed from the long composite core CHB14-2 (e.g., Schaebitz et al., 2021; Trauth et al., 2021; Foerster et al., 2022).

The RRMarch2021 age model works well when looking at climate changes on time scales longer than that of climate precession (~23 kyr), but larger uncertainties become evident when analyzing high-frequency climate fluctuations; this applies in particular in sections of the core younger than ~20 kyr BP and between 155 and 428 kyr BP (Roberts et al., 2021). Uncertainties in the younger section (<20 kyr BP) of the

* Corresponding author.
E-mail address: trauth@geo.uni-potsdam.de (M.H. Trauth).

https://doi.org/10.1016/j.qsa.2024.100208
Received 18 December 2023; Received in revised form 7 June 2024; Accepted 11 June 2024
Available online 21 June 2024

record are due to group of constraints in the AMS ^{14}C-based chronology of the younger section of CHB14-2 above ~10 m composite depth (mcd) (Roberts et al., 2021). Those constraints include a significant reduction in sediment accumulation rate between ~8.5 and 6.5 mcd corresponding to ~30 to 12 kyr BP (Roberts et al., 2021), which could also potentially be related to a hiatus or an erosional event. However, systematic offsets could also be due to contamination of the AMS ^{14}C ages in the upper part of the core, which would explain a set of ages being too young, or affected by an unknown reservoir effect, which would explain ages that are too old. Similar uncertainties, but not to this extent, have also been observed in the shorter cores CB01–06, but have been corrected by adaptive age-depth modeling that accounts for these offsets (Trauth et al., 2018). Using the RRMarch2021 age model a wide uncertainty interval opens up in the middle section (~155–428 kyr BP) of the long composite core, a common phenomenon in all age-depth models where the availability of numerical ages through direct dating is very limited. In the case of the RRMarch2021 age model this applies especially beyond the natural given saturation limit of the OSL method and the scarcity of ^{40}Ar/^{39}Ar dates and tephrochronological time markers below ~75 mcd (corresponding to ~155 kyr BP) and above ~234 mcd (corresponding to ~428 kyr BP) (Roberts et al., 2021).

A common way to bypass the constraints of a directly dated age model is orbital tuning (e.g., Hays et al., 1976; Pisias et al., 1984; Martinson et al., 1987). As a first attempt to use tuning techniques for the Chew Bahir record, we developed the multiband wavelet age modeling (MUBAWA) technique method (Duesing et al., 2021), which tracks the precession cycle through a wavelet power spectrum to account for possible variations in the sedimentation rate, but allows the selection of numerous parameters and therefore represents an interactive tuning technique. The adaptively tuned age model has many advantages when it comes to compensating for the limited age control of RRMarch2021 between ~75 and 234 mcd (corresponding to ~155–428 kyr BP). However, adaptive tracking of cycles in time series with an unfavorable signal-to-noise ratio could possibly lead to a fully reproducible, but sometimes ambiguous results. Keeping those caveats in mind, we will, however, use both the orbitally-tuned approach, as well as the RRMarch2021 age model based on direct dating, as a possible age models in our studies of the paleoclimate dynamics of the region, while being aware that all models are merely models (e.g., Blaauw and Heegard, 2012). This means that, at the very most, all age models can only represent an approximation of the true age-depth relationship in the sedimentary fill of the Chew Bahir basin (Trauth, 2014). However, since age models play a central role in paleoclimate studies, it is not surprising that the age-modeling methods used and the results of their application are always the subject of passionate discussions (e.g., Blaauw, 2010).

In this paper, we contrast the two published age models (RRMarch2021 by Roberts et al., 2021, and MUBAWA by Duesing et al., 2021) with a third model generated by a modern form of traditional tuning in three steps. First, an ensemble of traditionally tuned age models is generated, which differ in the choice of the initial base age. These age models are validated by numerical ages and a tephrochronological time marker as well as by the evolution of amplitudes in the time domain and frequency domain to identify a best tuned age model according to predefined quality criteria. Second, the middle part of the age model RRMarch2021 (i.e., between ~70 and 240 mcd) is replaced by the best tuned age model from the ensemble. Third, after merging the two age models, we replaced the proxy curve of the long composite core CHB14-2 with the corresponding curve of the short composite core CB01+03 and the associated AMS ^{14}C-based age model (Foerster et al., 2012; Trauth et al., 2018). This integrated composite age model provides an improved age control of the yet undated ~70–240 mcd interval of CHB14-2 and thus can contribute to make better use of high-frequency (shorter than the Earth's precession cycle) climate information from the Chew Bahir cores. We believe that the improved age model also helps to correlate the Chew Bahir environmental record with (usually likewise tuned) marine records, and, whilst recognising the limitations of (cross) spectral analysis of tuned age models in cause-and-effect studies, this also facilitates correlation with other terrestrial records of past climate change.

2. Setting, materials and methods

Chew Bahir is a tectonic basin, separated from the Lower Omo basin to the west by the Hammar Range, which is the main source of the sedimentary deposits at the coring sites (Fig. 1). Other important sediment sources for the detrital input are the Teltele Plateau to the east, the southwestern Ethiopian highlands to the north and the northern Rift lakes that have overflowed into Chew Bahir during lake high stands (Gebregiorgis et al., 2021). Being a closed basin, Chew Bahir forms a terminal sink for weathering products from its 32,400 km2 catchment. Between 2009 and 2014, we recovered several sediment cores of different lengths at Chew Bahir using different coring techniques. In late 2009 and 2010, six cores (CB01–06) were collected along a ~20 km long NW–SE transect across part of the basin (Foerster et al., 2012, 2015) (Table 1, Fig. 1). Datable material was identified in the CB01–06 short cores and comprised mostly biogenic carbonates and organic sediment, which were subsequently used for AMS ^{14}C dating (Foerster et al., 2012; Trauth et al., 2018). In May 2014, the ~40 m long core CHB14-1 was collected in the central most part of the Chew Bahir basin, not far from the location of core CB05 from the 2009–2010 coring campaigns, but 11.2 km southwest from the long cores CHB14-2A and 2B (Table 1, Fig. 1). The intermediate core CHB14-1 was dated using AMS ^{14}C dating of bulk sediment samples as suitable discrete biogenic material could not be identified, analyzing three samples, two of which were dismissed because they showed unexpectedly high δ13C values for bulk organic matter (>2.3‰) (Viehberg et al., 2018). Furthermore, polymineral fine

Table 1
Cored locations within the Chew Bahir basin (longitudes and latitudes), core lengths, total depth of cored material below the lake floor, date of core collection, and core recovery.

Core ID	Location	Latitude	Longitude	Length	Total Depth	Coring Date	Core Recovery
CB01	Margin	N 04°50.6'	E 36°46.8'	22 m	19 m	Dec 2009	81%
CB02	Margin	N 04°48.7'	E 36°46.2'	10 m	9 m	Nov 2010	97%
CB03	Intermediate	N 04°47.9'	E 36°47.2'	11 m	11 m	Nov 2010	98%
CB04	Centre	N 04°43.3'	E 36°50.2'	10 m	10 m	Nov 2010	99.5%
CB05	Centre	N 04°42.8'	E 36°51.3'	10 m	10 m	Nov 2010	97%
CB06	Centre	N 04°44.1'	E 36°47.9'	10 m	10 m	Nov 2010	97%
CB01–06		Composite Core			19 m		~95%
CHB14-1	Centre	N 4°42.4'	E 36°51.1'	37.89 m	40.69 m	Mar 2014	93%
CHB14-2A	Margin	N 4°45.7'	E 36°46.1'		278.58 m	Nov/Dec 2014	
CHB14-2B	Margin	N 4°45.7'	E 36°36.2'		266.38 m	Nov/Dec 2014	
CHB14-2		Composite Core			292.87 m		~90%

grain samples (4–11 μm) were extracted for luminescence dating and paleomagnetic dating was used (Viehberg et al., 2018).

The two parallel long cores CHB14-2A and 2B were collected in November–December 2014 about halfway along the CB01–06 transect (Table 1, Fig. 1). The 292.87 m long composite core with more than 90% recovery was developed by merging the two parallel cores 2A and 2B by core-to-core correlation using multi-sensor core logs, including color reflectance spectrometry (grayscale and 360–740 nm bands in 10 nm steps), core images, lithological description and X-ray fluorescence (XRF) data sets (Foerster et al., 2022). Age determinations for long cores CHB14-2A and 2B were based on AMS ^{14}C dating of ostracods, OSL dating of fine-silt sized quartz grains, and single-crystal total-fusion (SCTF) ^{40}Ar/^{39}Ar dating of feldspars from tuffaceous zones within the core. In addition, a volcanic ash layer identified in the core has been correlated on the basis of major and minor element geochemistry to a dated tephra found in the outcrop at Konso, in the southern Main Ethiopian Rift, namely the Silver Tuff (Roberts et al., 2021). The ages generated are stratigraphically consistent, and Bayesian age-depth modeling incorporating AMS ^{14}C, OSL and ^{40}Ar/^{39}Ar ages, and tephrochronological data has been used to build an age model for the Chew Bahir cores (age model RRMarch2021, Roberts et al., 2021; Vidal et al., 2022).

3. Age-depth modeling for the chew bahir cores

The short cores CB01–06, the intermediate core CBH14-1, and long composite core CHB14-2 were cored, dated, and analyzed independently in different laboratories. We used different dating techniques and age modeling algorithms to create age-depth models for the sediments (e.g., Foerster et al., 2012, 2015; Trauth et al., 2018; Viehberg et al., 2018; Duesing et al., 2021; Roberts et al., 2021).

In order to create an *age-depth model for the short cores CB01–06*, we first AMS ^{14}C dated 32 samples of organic sediment, fossilized charcoal, and biogenic carbonate extracted from cores CB01, CB03, CB05, and CB06 (Foerster et al., 2012, 2014, 2015; Trauth et al., 2015, 2018). The depths of the AMS ^{14}C dated samples in the individual cores were converted to a composite depth by an automatic inter-core correlation of the K curves of the cores CB01–06 using Dynamic Time Warping (Sakoe and Chiba, 1978; Paliwal et al., 1982; Trauth et al., 2018) (Fig. 2). In particular, the AMS ^{14}C ages from organic material and the AMS ^{14}C ages of the two cores CB05–06 from the centre of Chew Bahir show a strong scattering, which is why even sophisticated age modeling tools such as the *Bacon* software (Blaauw and Christen, 2011; Blaauw and Heegard, 2012) failed to provide a reasonable age model. We have therefore developed an age model in two steps. First, we selected those AMS ^{14}C ages that meet two criteria: We strictly used AMS ^{14}C ages measured on biogenic carbonate to avoid errors due to, for example, contamination of organic sediment (Fig. 2A), and we exclusively used ages from our

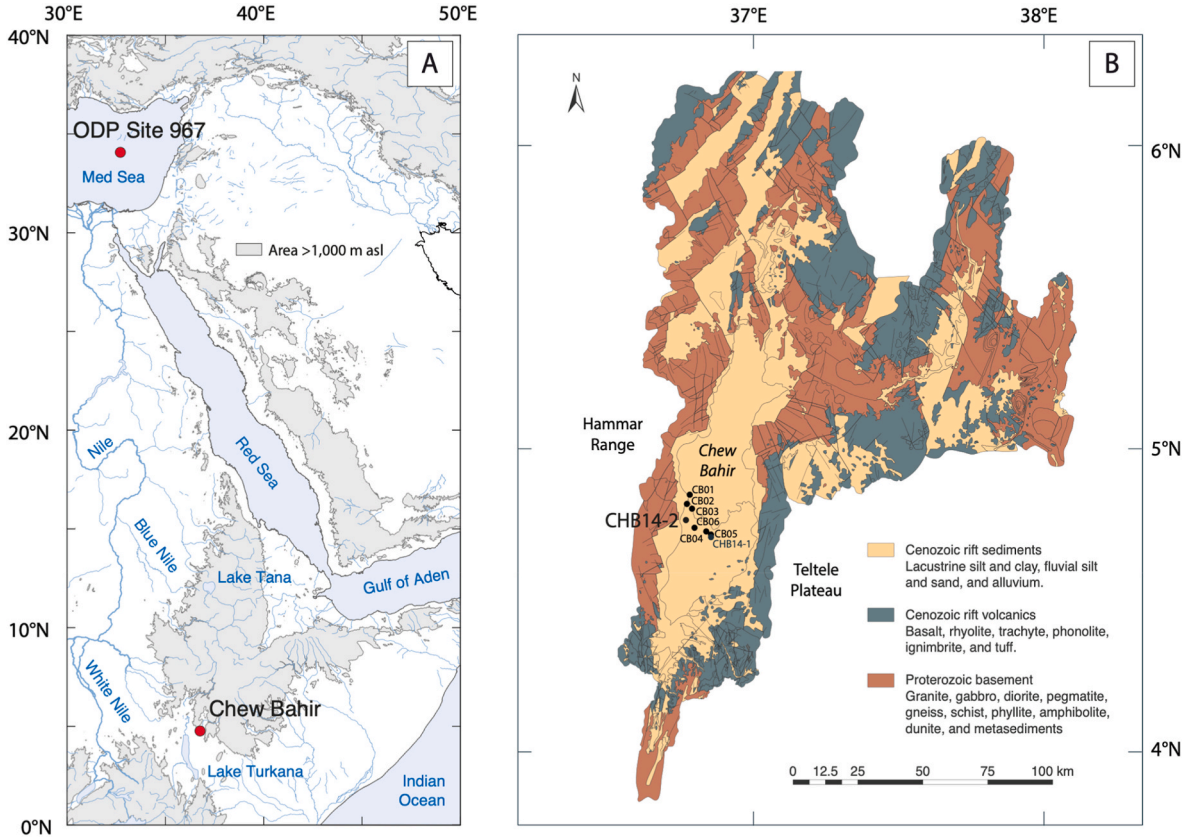

Fig. 1. (A) Map of northeastern Africa and adjacent areas showing the location of the Chew Bahir basin (4°45'40.55''N 36°46'0.85''E, ~500 m above sea level), the ODP Leg 160 Site 967 in the eastern Mediterranean Sea (34°4'6''N 32°43'31''E, ~2254 m water depth), and the river Nile with its two tributaries the White and Blue Niles connecting both regions (modified from Trauth et al., 2019). Coastline and river polygons from the Global Self-consistent, Hierarchical, High-resolution Geography Database (GSHHG) (Wessel and Smith, 1996). Topography from the 1 arc-minute global relief model of the Earth's surface (ETOPO1) (Amante and Eakins, 2009). (B) Geologic map of the Chew Bahir basin, showing the four generalized rock types: Quaternary rift sediments, Neogene and Paleogene rift volcanics, and Paleozoic–Proterozoic basement, and the location of the short cores CB01–06, the intermediate core CHB14-1 and the long cores CHB14-2A and 2B. Compilation based on Omo River Project Map (Davidson, 1983), Geology of the Sabarei Area (Key, 1988), Geology of the Yabello Area (Hailemeskel, 2004), and Geology of the Agere Maryam Area (Hassen, 1997) (modified after Trauth et al., 2018). (For interpretation of the references to color in this figure legend, the reader is referred to the Web version of this article.)

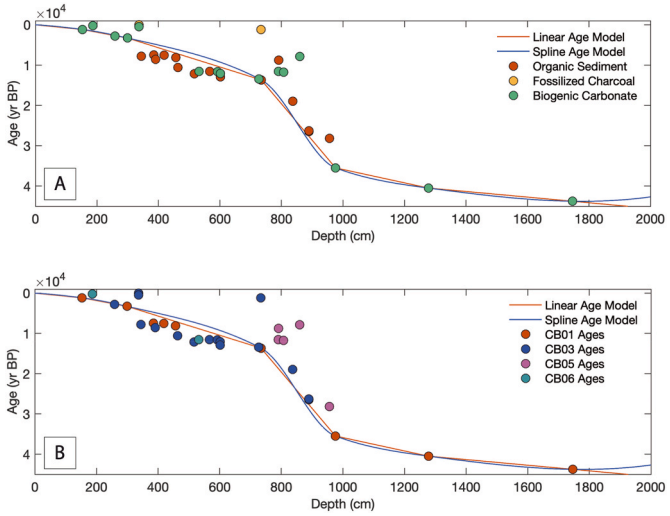

Fig. 2. Linear (red) and cubic spline (blue) age models of the short cores CB01–06 based on 32 AMS ^{14}C ages (from Foerster et al., 2014), originally converted to calibrated ages using IntCal13 (Reimer et al., 2013), now calibrated using the IntCal20 curve (Reimer et al., 2020). The AMS ^{14}C ages are colored according to (A) the type of dated material or (B) the origin of the dated material from the respective short core CB01, CB03, CB05 and CB06. The AMS ^{14}C ages show a significant scatter for various reasons, which is why a comparatively simple (linear) age model was preferred (see Trauth et al., 2015, 2018 for a detailed discussion of the age model of the short cores CB01–06). (For interpretation of the references to color in this figure legend, the reader is referred to the Web version of this article.)

longest CB01 core with by far the best XRF record and to avoid errors in the inter-core correlation of the samples Fig. 2B). The attempt to detect and quantify a possible reservoir effect was not successful: a single sample of charcoal in core CB03 was much too young (Fig. 2A). However, the scattered ages of organic material, which are consistent with the ages of biogenic carbonate, suggest a very small, if any, reservoir effect. Second, we used a stepwise linear interpolation technique to create an age-depth model from six AMS ^{14}C ages that fulfil the two criteria; for comparison, a spline interpolation method was used to create an alternative age-depth model, which deviates only slightly from the stepwise linear age model (Fig. 2A and B). The sedimentation rates of the age model are between 50 and 70 cm/kyr during periods of wetter climate (<15 kyr and >35 kyr BP), which frame a period of drier climate with sedimentation rates of ~10 cm/kyr (~15–35 kyr BP). The resolution of the geochemical and physical data sets leads to a resolution of the climatic history of ~3–12 years, which allows us to make estimates concerning the abruptness of trends and events in climate, even though the core section older than ~20 kyr BP with only a few AMS ^{14}C ages and close to the limit of the dating method makes it increasingly difficult to date these events (Trauth et al., 2015, 2018, 2024).

A *first age-depth approximation for the intermediate core CHB14-1* was based on AMS ^{14}C ages, luminescence dates of polymineral fine-grains using a post-IR IRSL signal and the results from paleomagnetic measurements (Viehberg et al., 2018). These age control points were iteratively shifted within the error of the individual ages to fit general patterns in our relative paleointensity (RPI) record with regional RPI data from the Somali Basin (Meynadier et al., 1995). To further refine our age model, we correlated minima and maxima in our RPI record to available paleomagnetic data from Chew Bahir (Trauth et al., 2015, 2018), the high resolution global relative paleointensity stack (GLOPIS, Laj et al., 2013), and the RPI data from ODP Site 984 (Channell et al., 2002) from the Iceland Basin. The final age-depth model is based on one AMS ^{14}C age, nine luminescence dates and three tie-points derived from the correlation of RPI record. A Bayesian model approach was used to determine the most likely age-depth curve using the *Bacon* software (Blaauw and Christen, 2011) and the INTCAL13 data set (Reimer et al., 2013). A dynamic setting was presumed for the sediment accumulation rates and a step size of 15 cm segments was chosen to estimate the ages. The age-depth model reveals a mean sedimentation rate of ~46 cm/kyr in the interval 40.68–13.70 m, relative to a mean sedimentation rate of ~25 cm/kyr in the top part (Viehberg et al., 2018).

As a result of the variety of individually dated cores and application of different modeling approaches we can draw on several *different age models for the composite long core CHB14-2* (Figs. 4–6, Suppl. Figs. 1–3). All four age models have their strengths and weaknesses, but are generally in good agreement: (1) a directly dated age model RRMarch2021 with a yet undated middle part between ~75 and 234 mcd (corresponding to 155–428 kyr BP) (Roberts et al., 2021), (2) an adaptively tuned age model using a new multiband wavelet age modeling (MUBAWA) technique (Duesing et al., 2021), (3) a suite of traditionally tuned age models MHT450–650 with different initial base ages (this work), and (4) a combined composite age model that uses the CB01+03 age model from the short cores for the top <20 kyr BP interval, the RRMarch2021 age model for the 20–150 kyr BP and >451 kyr BP intervals and the MHT560 age model for the as yet undated 150–451 kyr BP interval (this work). The four age models differ in (1) the agreement with established chronologies of the last ~20 kyr including the timing of the African Humid Period (AHP) and the dry episode during the Younger Dryas Stadial (YDS), (2) the middle part of the core

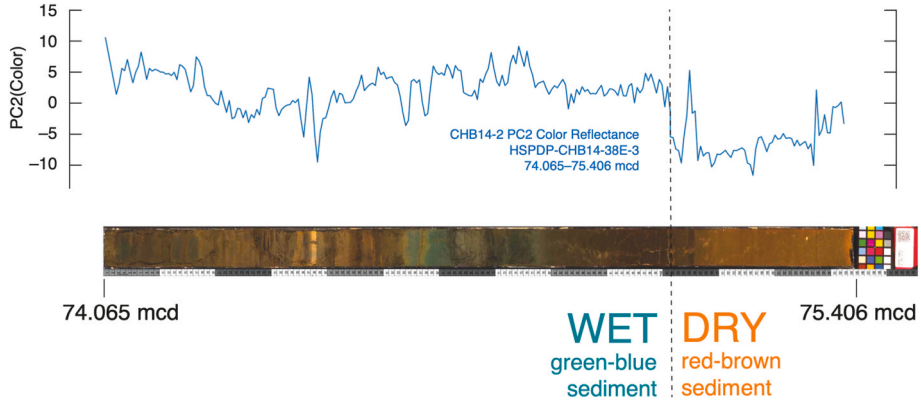

Fig. 3. Sediment color information as a proxy for water level fluctuations. The 2nd principal component (PC2) of color reflectance values (upper panel) describes the change from green-blue to red-brown sediment. This color change reflects the oxidation state of the iron (pyrite vs. iron hydroxide), which in turn is a reflection of the fluctuating aeration of the water body and the sediment in the course of lake level fluctuations. The PC2 of the color reflectance values indicate positive values during episodes of a wetter climate, and negative values when it was dry (Duesing et al., 2021). (For interpretation of the references to color in this figure legend, the reader is referred to the Web version of this article.)

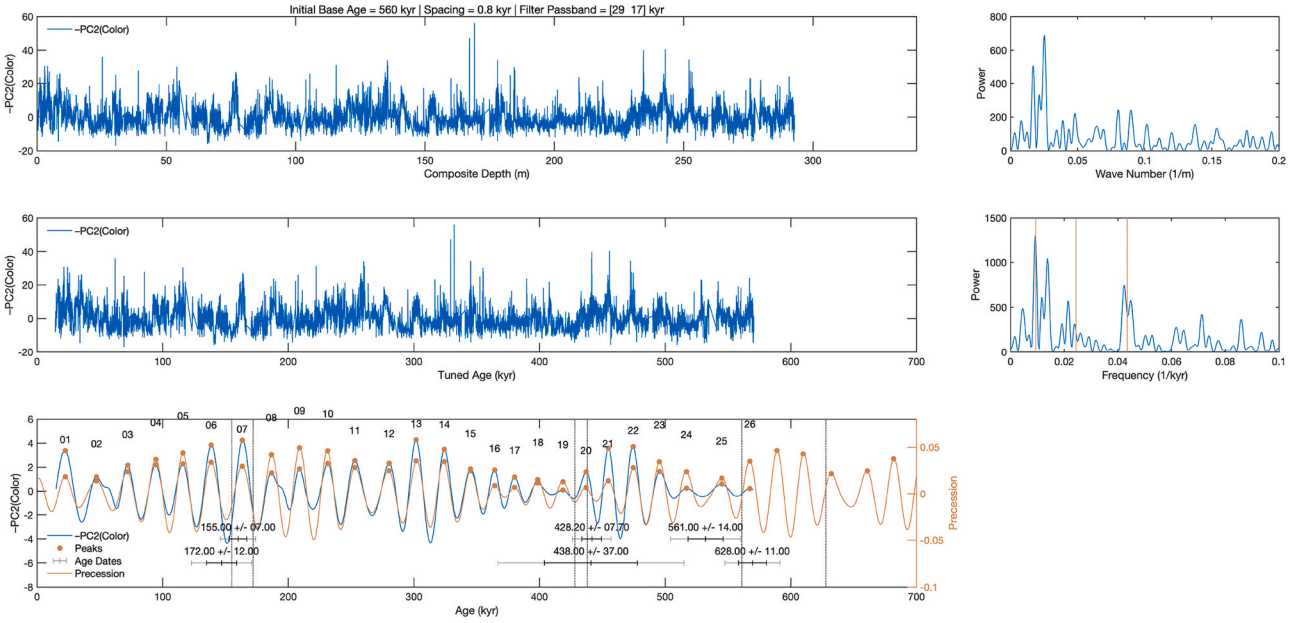

Fig. 4. Result from tuning the negative 2nd principal component (PC2) of color reflectance values to climate precession using an initial base age of 560 kyr BP of composite Chew Bahir core CHB14-2. The negative 2nd principal component (PC2) of color reflectance values with changed sign (upper left panel). The negative PC2 tuned to orbital precession (middle left panel); since the PC2 of the color reflectance values indicate positive values during episodes of a wetter climate we have to change the sign of PC2 before tuning maximum PC2 to maximum precession causing a drier climate in eastern Africa. The bandpass-filtered negative PC2 (blue) tuned to orbital precession (orange) according to Laskar et al. (2004) together with $^{40}Ar/^{39}Ar$ ages shown as one-sigma (thin black lines) and two-sigma (thick black lines) error bars according to their respective tuned ages, but labeled according to their actual numerical ages and one-sigma errors and at their actual position along the *x*-axis (dotted vertical lines) (lower left panel). Lomb-Scargle powerspectra (with the fundamental orbital cycles 106 kyr, 41 kyr and 23 kyr marked as vertical lines) of the negative PC2 of the color reflectance values record before (upper right panel) and after tuning to validate the tuning result (lower right panel). (For interpretation of the references to color in this figure legend, the reader is referred to the Web version of this article.)

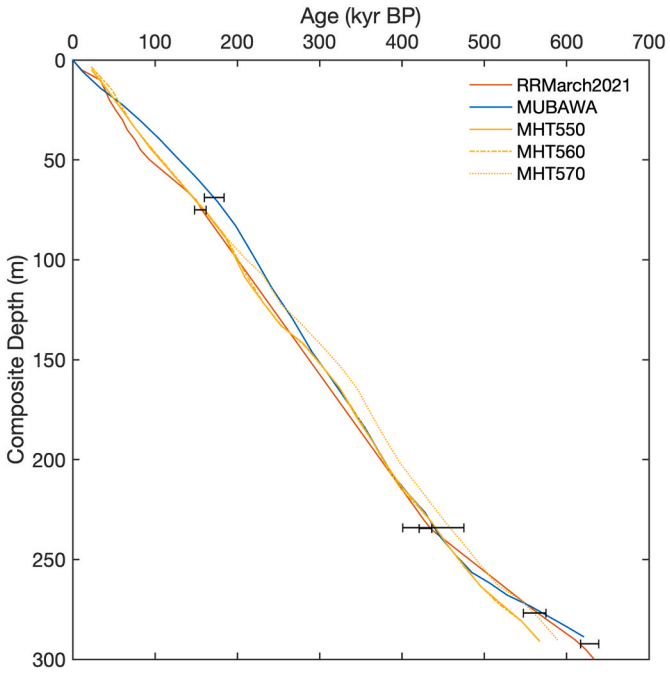

Fig. 5. Age-depth plots of the age models RRMarch2021 (Roberts et al., 2021), MUBAWA (Duesing et al., 2021) and MHT550, 560 and 570 (this work) of composite Chew Bahir core CHB14-2. Black symbols mark the age of the Silver Tuff (with one-sigma error) and the $^{40}Ar/^{39}Ar$ ages (with one-sigma errors).

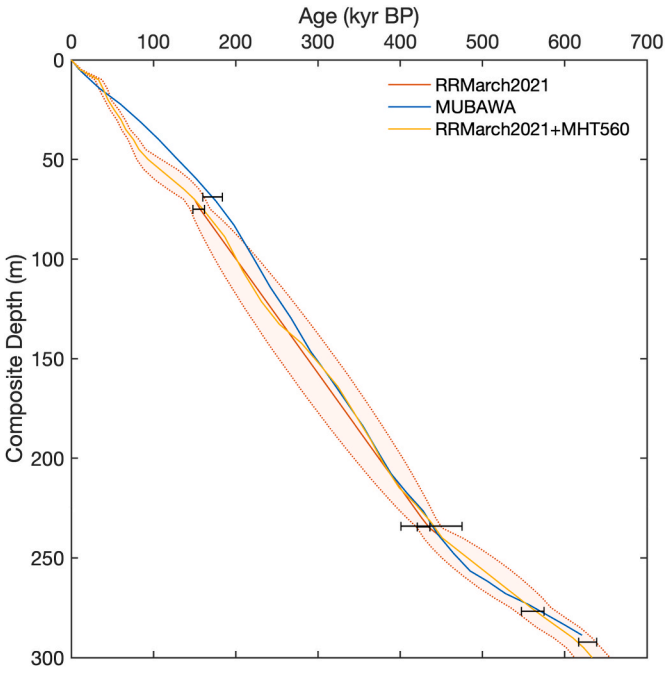

Fig. 6. Age-depth plots of the age models RRMarch2021 with 95% confidence bounds (Roberts et al., 2021), MUBAWA (Duesing et al., 2021) and the merged age models RRMarch2021+MHT550 and RRMarch2021+MHT560 (this work) of composite Chew Bahir core CHB14-2. Black symbols mark the age of the Silver Tuff (with one-sigma error) and the $^{40}Ar/^{39}Ar$ ages (with one-sigma errors).

between ~70 and 240 mcd (corresponding to 150–451 kyr BP according to Roberts et al., 2021) where there is no direct dating available and (3) in the influence of the two oldest $^{40}Ar/^{39}Ar$ ages, 561 ± 14 kyr BP and 628 ± 12 kyr BP old, respectively, at the core base (at ~277 and ~292 mcd, respectively) (Fig. 7).

Our *first age model* RRMarch2021 (Roberts et al., 2021) used to provide a first chronology for the Chew Bahir composite core is based exclusively on AMS ^{14}C, OSL and $^{40}Ar/^{39}Ar$ ages, and tephrochronological data (Fig. 5, Suppl. Fig. 2 + 3). A Bayesian age-depth model was created using OxCal v4.4.3 (Bronk Ramsey, 2017) using the Poisson P_Sequence model (Bronk Ramsey, 2008) which assumes an underlying random process of deposition which is uniform over long timescales. The age of the top of the sequence was fixed to 2014 CE, the year of coring. The AMS ^{14}C dates were calibrated within OxCal using the IntCal20 calibration curve (Reimer et al., 2020); prior to this, allowance was made within the model for an unknown reservoir effect of between 0 and 3000 years, giving a single reservoir offset value determined from the examination of multiple age determinations through the modeling process, applied to the AMS ^{14}C ages prior to calibration. The time range described by the absolute precision (i.e., the span of the 95% confidence intervals expressed in kyr) of the RRMarch2021 age model increases with increasing depth, with a maximum in absolute values of ~30 kyr window at 50 mcd and 20–70 kyr below 50 mcd (Roberts et al., 2021).

Our *second age model* MUBAWA (Duesing et al., 2021) used a new multiband wavelet age modeling (MUBAWA) technique (Fig. 3 + 5, Suppl. Fig. 2 + 3). In contrast to traditional tuning methods, which use a single, defined bandpass filter, this new method used an adaptive bandpass filter that adapts to changes in continuous spatial frequency evolution paths in a wavelet power spectrum, within which the wavelength varies considerably along the length of the core due to continuous changes in long-term sedimentation rates. For this new tuning approach Duesing et al. (2021) used the 2nd principal component (PC2) of color reflectance values from the sediment (Fig. 3). Those PC2 values showed distinct cycles with wavelengths of 10–15 m and of ~40 m that can be attributed with a high likelihood to the influence of orbital cycles. The MUBAWA model in Duesing et al. (2021) comprised five independent $^{40}Ar/^{39}Ar$ ages from volcanic ash layers that were identified within the core plus a tephrochronological time marker identified in the core that has been correlated on the basis of major and minor element geochemistry to a dated tephra found in the outcrop at Konso, in the southern Main Ethiopian Rift, namely the Silver Tuff (Roberts et al., 2021) to determine an approximate spatial frequency range for the orbital signal. The MUBAWA age model has not been used in any other publication to date, as the directly dated age model RRMarch2021 became available at the time of publication of the former.

Our new and *third age model*, first presented here, uses a MATLAB algorithm based on traditional tuning that was developed in paleoceanography in the late 1970s (e.g., Hays et al., 1976; Pisias et al., 1984; Martinson et al., 1987) (Fig. 3 + 5, Suppl. Figs. 1–3). The algorithm first creates a preliminary age model by linear interpolation between a top age of 0 kyr and a base age of the core based on $^{40}Ar/^{39}Ar$ age dates. It then bandpass-filters, as an example, the PC2 of the color reflectance values as in MUBAWA tuning, to extract the frequency band of climate precession (0.0345–0.0588 kyr–1, corresponding to periods of 17–29 kyrs). The algorithm then automatically tunes the maxima of the filter output to the maxima of the precession according to Laskar et al. (2004) using the findpeaks algorithm from the Signal Processing Toolbox of MATLAB. The PC2 of the color reflectance values indicate positive values during episodes of a wetter climate, and negative values when it was dry (Duesing et al., 2021). Since the climate in eastern Africa is humid during the precession minima/northern hemisphere insolation maxima (e.g., Schaebitz et al., 2021; Foerster et al., 2022), we need to change the sign of the PC2 before we tune the bandpass-filtered PC2 maxima to the precession maxima. To validate the results, we first checked the Lomb-Scargle spectra of the original PC2 of the color reflectance values before and after tuning to ensure that the amplitude of

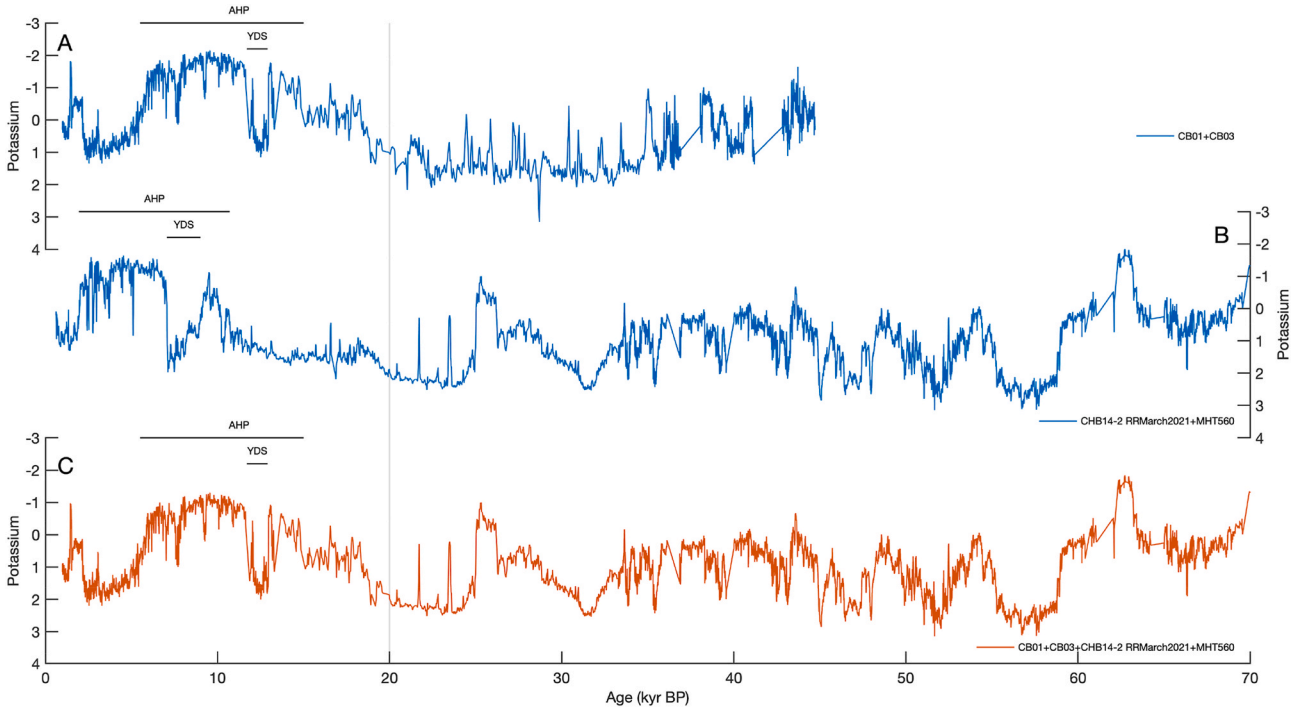

Fig. 7. Result from merging the normalized K record of the composite short core CB01+03 and composite long core CHB14-2 from the Chew Bahir using the RRMarch2021+MHT560 age model (this work). (A) Normalized K record of the composite short core CB01+03 (Foerster et al., 2012; Trauth et al., 2018). (B) Normalized K record of the composite long core CHB14-2 using the RRMarch2021+MHT560 age model (this work). (C) Normalized K record of the CB01+03 and CHB14-2 with chronologies merged at 20 kyr (marked by vertical gray line) after adjusting the potassium record of CB01+03 in order to seamlessly connect to the potassium record of CHB14-2, using younger-most part of the much more detailed CB01+03 chronology and the older part of the RRMarch2021+MHT560 chronology.

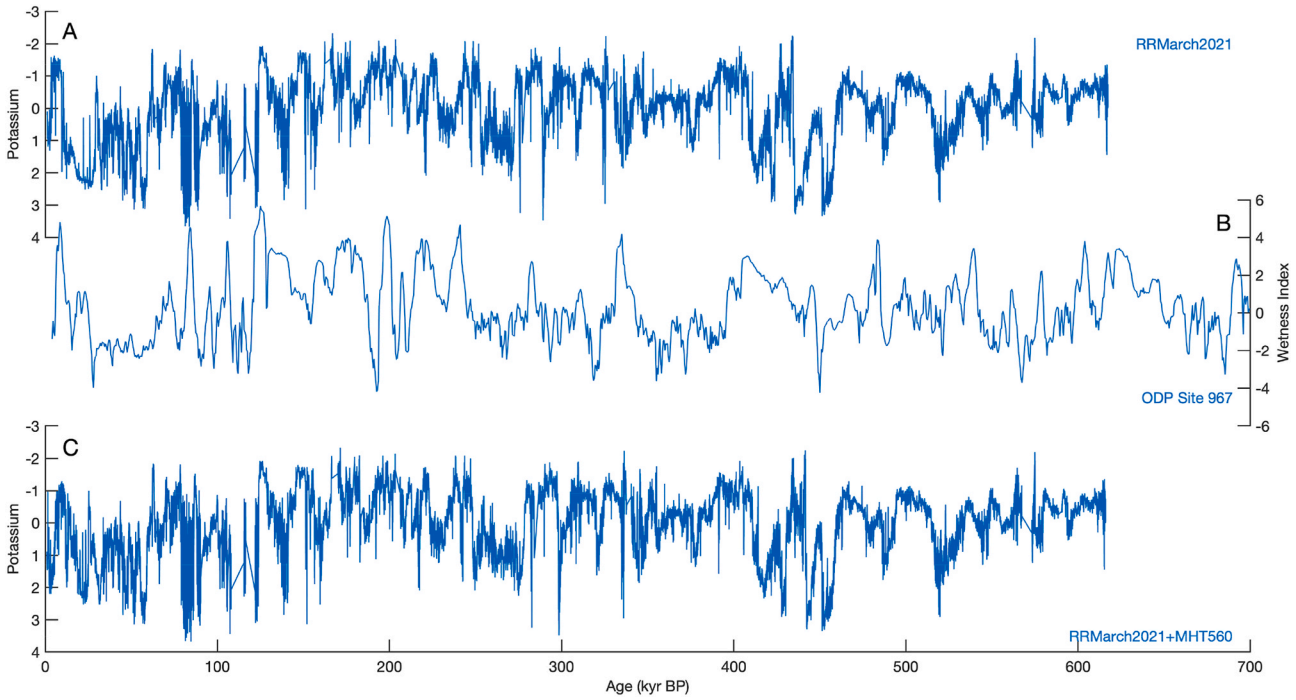

Fig. 8. Correlating the normalized potassium record from composite Chew Bahir core CB01+30 and CHB14-2 using the age models RRMarch2021 (Roberts et al., 2021) (upper panel) and RRMarch2021+MHT560 (this work) (lower panel) with the wetness index of ODP Site 967 (Grant et al., 2017).

the orbital eccentricity does not decrease during tuning to climate precession. Secondly, we checked the consistency of the age model with the $^{40}Ar/^{39}Ar$ ages 172 ± 12 kyr BP, 428.2 ± 7.7 kyr BP, 438 ± 37 kyr BP, 561 ± 14 kyr BP, and 628 ± 12 kyr BP, as well as the correlated age of the 155 ± 7 kyr BP Silver Tuff (Roberts et al., 2021). Third, we compared the course of the amplitudes of the bandpass-filtered PC2 through time compared to climate precession. Finally, the proxy record of interest, such as the potassium (K) record, is adjusted to this age model using a piecewise shape-preserving cubic Hermite interpolation using the MATLAB function pchip (Frisch and Carlson, 1980; MathWorks, 2023).

In tuning experiments there are generally two main parameters that can be changed (Fig. 4, Suppl. Fig. 1). First, the width of the filter, where in this case a 17–29 kyrs passband proved to be a good compromise when it came to taking into account the potentially strongly fluctuating sedimentation rates, on the other hand to generate a filtered signal that no longer bears any resemblance to the observed 10–15 m and of ~40 m cyclicities in the color reflectance values. Second, the initial base age, which provides a rough age estimate for the sediment and is thus a prerequisite for successful interpolation and bandpass filtering prior to tuning. In marine tuning projects, reversals of the earth's magnetic field are used, such as the Brunhes–Matuyama magnetic polarity reversal (~773 kyr BP, Singer et al., 2002). Unfortunately, this event could not be detected in the composite core CHB14-2, so we used the two oldest $^{40}Ar/^{39}Ar$ ages 561 ± 14 kyr BP, and 628 ± 12 kyr BP as a rough estimate of the age of the core base. We therefore ran the algorithm with base ages from 450 to 650 kyr BP in 10 kyr increments based on the $^{40}Ar/^{39}Ar$ dating results to check the results according to the two methods for validation (Suppl. Fig. 1). From the 21 different tuning experiment results MHT450–650 we picked the MHT550, MHT560, and MHT570 as the best age models based on our criteria described above (Suppl. Table 1). Overall, these age models show a very similar course as the other two age models RRMarch2021 and MUBAWA, but with deviations in detail (Fig. 5, Suppl. Fig. 2 + 3). The age models RRMarch2021, MHT550, MHT560, and MHT570 run parallel in the upper part of the composite core, with the exception of a kink in RRMarch2021 at ~10 mcd, whereas MUBAWA is generally older by approximately one precession cycle. Below ~75 mcd, MHT570 is older than RRMarch2021, MHT550, and MHT560 by about the same amount. The most significant difference occurs below ~240 mcd where the RRMarch2021 and MUBAWA try to catch the two oldest $^{40}Ar/^{39}Ar$ ages while the MHT550 and MHT560 age models do not. MHT570 agrees with the younger age of the two $^{40}Ar/^{39}Ar$ ages but fails to catch the oldest $^{40}Ar/^{39}Ar$ age. As a consequence, the base of the core at ~290 mcd is ~570 kyr old according to MHT550 and MHT560, and ~590 kyr according to MHT570, whereas the two other age models RRMarch2021 and MUBAWA reach base ages in the order of ~620–630 kyr.

Our *fourth age model*, also first presented here, is a complementation of the RRMarch2021 age model with the MHT560 age model (Fig. 6, Suppl. Fig. 2 + 3). We combine these two age models because they agree well and especially in the transition regions at ~70 mcd (corresponding to ~150 kyr BP) and at ~240 mcd (corresponding to ~451 kyr BP), where both models fit seamlessly, whereas the MUBAWA and MHT570 age models are ~20 kyr older at this point. The age models MHT550 and MHT560 are very similar, but bandpass filtered PC2 of MHT560 has slightly higher amplitudes in the interval between 150 and 451 kyr BP than MHT550 (Suppl. Figs. 1K and L, lower panels), which is why we decided in favour of MHT560. The age model RRMarch2021+MHT560 combines the advantages of the RRMarch2021 age model that is more detailed above 70 mcd and the more detailed age model MHT560 below that depth where there is limited direct dating control. A combined age model also solves the problem that the tuned age models are unable to reach the two oldest $^{40}Ar/^{39}Ar$ ages and thus represent a probable halving of the sedimentation rate below ~240 mcd. The age model RRMarch2021+MHT560, however, fails in trying to produce a good chronology for the core section younger than ~20 kyr BP (Fig. 7). The two age models tuned at the precession cycle do not provide detailed age information for the core section younger than ~20 kyr BP. In contrast to the K record of the short cores CB01+03 (Fig. 7A), the K record using the RRMarch2021+MHT560 age model suggests that the ages for the AHP (15–5 kyr BP) and the dry episode at the time of the YDS (~12.7–11.6 kyr BP) are systematically too young by ~4 kyrs (Fig. 7B). On the other hand, the chronology of CB01+03 cores older than ~20 kyr is subject to large uncertainties (Trauth et al., 2015, 2018). We therefore first

recalibrated the AMS ^{14}C ages of the short cores (from Foerster et al., 2014), originally converted to calibrated ages using IntCal13 (Reimer et al., 2013), using the IntCal20 curve (Reimer et al., 2020). We then recalculated the linear age model by running the corresponding MATLAB script without any further modifications, but with the recalibrated AMS ^{14}C ages. Finally, we adjusted the values of the potassium record of CB01+03 near the transition at 20 kyr before stitching the two curves together (Fig. 7C). This enables us to seamlessly connect to the potassium record of the fully continuous, well studied high resolution potassium record of the short cores CB01+03 with CHB14-2, using the younger-most part of the more detailed CB01+03 chronology and the older part of the RRMarch2021+MHT560 chronology.

4. Discussion

The published age model RRMarch2021 provides the maximum level of accuracy on long time scales in large parts of composite core CHB14-2 with the available directly dated material, but shows larger uncertainties in the sections of the record younger than ~20 kyr BP and between ~155 and 428 kyr BP. The 95% confidence bounds are about two precession cycles wide, e.g., ages ranging from 100 to 145 kyr BP at 60 mcd and between 250 and 320 kyr BP at 150 mcd (Roberts et al., 2021) (Fig. 6 + 7, Suppl. Figs. 4–7). The lack of precision occurs because this section of the core is too old to be dated using AMS ^{14}C or OSL dating and no dateable or correlateable tephra occur between 75 and 234 mcd (Roberts et al., 2021). We therefore tested and applied two different methods of orbital tuning to calculate an improved age model: multiband wavelet age modeling (MUBAWA) (Duesing et al., 2021) and traditional tuning (e.g., Hays et al., 1976; this work). In a second step, a combined age model or proxy record is generated for the Chew Bahir, which consists of the continuous and high resolution short core composite CB01+03 (Foerster et al., 2012, 2015; Trauth et al., 2015, 2018) and their corresponding age model in the section <20 kyr BP. In the interval between 20 and 150 kyr BP, the proxy record consists of the data from the long composite core CHB14-2 with the RRMarch2021 age model that is especially in this interval well-constrained by a series of OSL dates (Roberts et al., 2021). Between ~150 and 451 kyr BP kyr BP, i.e., beyond the saturation limit of OSL dating, we use the proxy record from the long composite core CHB14-2, but the orbitally tuned age model MHT560 (this work). Below ~451 kyr BP, where suitable material for ^{40}Ar/^{39}Ar dating provides direct ages, we use CHB14-2, but again with the RRMarch2021 age model (Roberts et al., 2021). The resulting climate record goes back to ~620 kyr BP (Roberts et al., 2021; Foerster et al., 2022).

Comparing the RRMarch2021, MUBAWA and RRMarch2021+MHT560 age models in the time domain, significant shifts in PC2 of the color reflectance values become apparent, as could be expected looking at the age-depth graphs (Suppl. Figs. 4–8). Comparing the actual age (and 1-sigma error) of the ^{40}Ar/^{39}Ar dated samples with the age of the corresponding composite depth as predicted by the respective age models, there are sometimes significant discrepancies (Fig. 5 + 6). Again, this was expected, as the samples are quite close to each other in pairs, but differ significantly in their numerical age. This is particularly true at the base of the composite core, where two ages from samples, ~15.4 mcd apart, are very different in terms of age (~67 kyrs), even with the error bar of 11 kyr and 14 kyr, respectively, taken into account. The RRMarch2021 and MUBAWA age models, after incorporating the younger of the two ages, try to (almost) hit the older age as well. This succeeds only if the sedimentation rate to the core base decreases dramatically, which the tuned age models MHT550–570 do not show, in contrast to the other age models including RRMarch2021+MHT560. Due to the different model behavior toward including/excluding ^{40}Ar/^{39}Ar ages, which differ significantly although being situated only a few meters apart in the core, the age models differ greatly at the base of the composite core: The MHT550–570 age models determines a maximum age of ~570–590 kyr BP, while RRMarch2021 calculates a maximum age of ~617 kyr BP at the base of the composite core (293 mcd), MUBAWA even estimates ~636 kyr BP.

There are also clear variations in the region around 150–170 kyr BP, where an age reversal in the ^{40}Ar/^{39}Ar ages occurs: here, a sample with an age of 172 ± 12 kyr BP lies above the Silver Tuff with a correlated age of 155 ± 7 kyr BP (although the ages agree within 1-sigma errors) (Fig. 5 + 6). Unfortunately, this age range also falls beyond the upper age limit of the quartz OSL method where dated mineral grains reach saturation and are unable to generate reliable finite ages at this site (Roberts et al., 2021). Correspondingly, the color reflectance curves here also deviate from each other by several tens of thousands of years (Suppl. Figs. 4–8). In the other parts of the core, the age models are generally one to two precession cycles apart, and tuning certainly helps to compensate for the missing information of the RRMarch2021 age model in the ~75–235 mcd section of the core. The advantage of tuning can also be seen in the quality of the Lomb-Scargle spectra, where MUBAWA is not expected to have a stationary eccentricity cycle due to the time-varying tracking of the precession cycle (Fig. 9, Suppl. Fig. 1 + 8). In the case of the tuned age models MHT550–570, it is no surprise that the spectra of the tuned data show a clear eccentricity cycle, as the strength of this cycle is one of the criteria for selecting the best out of the 21 possible tuned age models. In the RRMarch2021+MHT560 age model, the precession cycle is clearly evident, but the eccentricity cycle (very evident in the Lomb-Scargle spectrum of the PC2 of the color reflectance values with the MHT560 age model) has largely disappeared. This is the result of mixing a directly dated (non-tuned) age model above ~70 mcd and below ~240 mcd with the tuned MHT560 age model.

Unfortunately, as always with age models, there is no indication which of the calculated age models is closest to true age-depth relationships (e.g., Bronk Ramsey, 2008; Blaauw and Christen, 2011; Trauth, 2014). All three age models are the best age model given the assumptions made, e.g., that a linear relationship exists between the PC2 of color reflectance values and climate precession (Duesing et al., 2021). Additional age determinations or tephrochronological time markers can potentially provide further information, but these – as well as all existing ages – have unknown systematic errors (e.g., Lowe, 2011). In addition to these systematic errors, there are random errors which influence the precision of an age, for example due to the sometimes very small sample size for the ^{40}Ar/^{39}Ar ages (Roberts et al., 2021). Random errors are a possible explanation for the observed inconsistencies, for example, between ^{40}Ar/^{39}Ar dating and tephrochronology. The correlation with other climate time series could potentially provide useful additional information, but holds the risk of importing new uncertainties from other chronologies and, as expected, should record similar regional climate signals. Unfortunately, even all these climate time series have uncertainties in their age models, and marine records in particular are usually likewise tuned. Therefore, correlation (or the absence of correlation) is not necessarily indicative of the accuracy of a particular model for the Chew Bahir cores.

One climate time series that might meet at least some of the requirements is the well established wetness index record of ODP Site 967 (Grant et al., 2017) (Fig. 1 + 8, Suppl. Figs. 4–7). According to the authors this index reflects pan-African Humid Periods, i.e., large-scale climate trends in north, northwest and eastern Africa, which includes the Ethiopian highlands and therefore possibly also the Chew Bahir site (Grant et al., 2017; Trauth et al., 2019). Of course, it may be that actual differences in climate result in a weak correlation, however similar but time-shifted curves provide important clues to possible errors in the age model. Comparing the K curve from Chew Bahir with the wetness index from ODP Site 967, the normalized K record with the RRMarch2021+MHT560 age model shows a much better correlation on time scales shorter than the 1–2 precession cycles, where the RRMarch2021 age model shows little or no correlation. Smaller deviations on shorter time scales (less than one precession cycle) are nevertheless possible, partly because of the rather wide bandpass (16–28

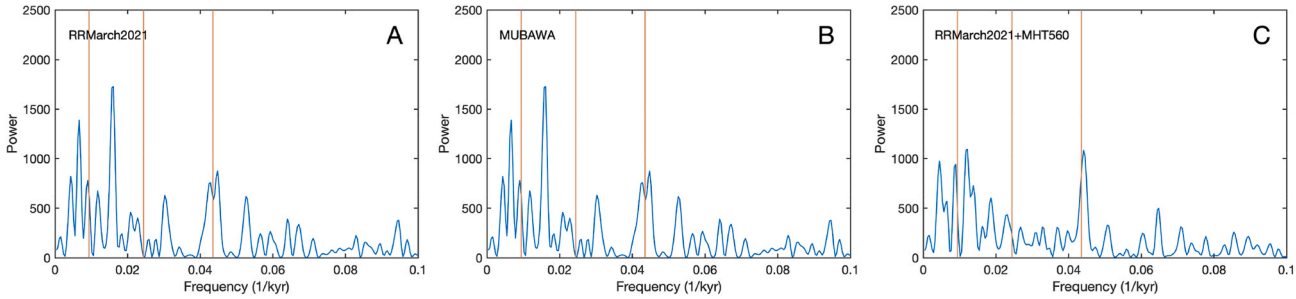

Fig. 9. Comparing the Lomb-Scargle powerspectra of the PC2 of the color reflectance values adjusted to the age models (A) RRMarch2021 (Roberts et al., 2021), (B) MUBAWA (Duesing et al., 2021) and (C) the merged age model RRMarch2021+MHT560 but with the K record of CHB14-2 being replaced by the potassium record of CB01+03 (this work). (For interpretation of the references to color in this figure legend, the reader is referred to the Web version of this article.)

kyr) of the filter used for orbital tuning, and partly because they do actually occur in nature and could reflect real shifts. In this context, it should be noted that the PC2 of color reflectance values was tuned, not K concentrations, which reflect local authigenic and post-sedimentary illitization of smectites in the sediment in the course of increasing pore water alkalinity (Foerster et al., 2018; Gebregiorgis et al., 2021; Arnold et al., 2021). Particularly striking is the very similar pattern of the time series of the Chew Bahir site and the ODP Site 967, recorded ~3300 km apart, during a prolonged dry period between 280 and 245 kyr BP, but also at other times in the past such as around 450 kyr BP. The abrupt wet-dry transition at ~120 kyr BP appears concurrently, as expected, since the K record with the RRMarch2021+MHT560 age model and with the RRMarch2021 age model are identical between 20 and 150 kyr BP and use the same age model RRMarch2021, similar to the K record older than 450 kyr BP.

Looking at the temporal variation of the Spearman correlation coefficient between the K curve from Chew Bahir, adjusted to one of the three age models RRMarch2021, MUBAWA and RRMarch2021+MHT560, and the wetness index of ODP Site 967, differences in detail become obvious (Suppl. Figs. 4–7). Using a moving window with a width of 500 data points corresponding to 50 kyr, negative values for the correlation coefficient mean a positive correlation with respect to moisture, since negative values for the K proxy mean wetter conditions at Chew Bahir, whereas positive values of the wetness index mean wetter conditions at ODP Site 967. The correlation between Chew Bahir using the RRMarch2021 age model and ODP Site 967 is high in the range <140 kyr BP and >440 kyr BP, and also between 260 and 280 kyr BP and at around 380 kyr BP (Suppl. Fig. 4). The high correlation between 260 and 280 kyr BP is due to an agreement during the dry episode between 240 and 280 kyr BP although the two records are not in phase regarding the onset and termination of this episode. The correlation centered at 380 kyr BP is primarily due to the coincidence of a short-term wet-dry-humid cycle during this time interval. The correlation between the K curve and the wetness index is very weak when using the MUBAWA age model (Suppl. Fig. 5). A stronger correlation is found in the range between 130 and 190 kyr BP and 370–430 kyr BP, the latter of which is also visible in the other age models.

The age model RRMarch2021+MHT560 shows a very balanced correlation, which is mainly due to the good correlation in the long wavelength (up to 1–2 precession cycles), except for the section older than ~550 kyr BP where we use the RRMarch2021 age model (Suppl. Fig. 6 + 7). In this time interval, the tuning result fits well, also the validation by the $^{40}Ar/^{39}Ar$ ages shows a good fit. Thus, the difference between the ODP Site 967 wetness index record and the CHB14-2 normalized K record in that interval could be due to actual climatic differences between the two localities. On the other hand, the two records actually show striking similarities, in the way that the section between 520 and 580 kyr BP in CHB14-2 looks very similar to the section between 560 and 620 in ODP Site 967, but shifted by two precession cycles. Assuming that the tuned age model of ODP Site 967 is correct, this would mean that the two (partially contradictory) $^{40}Ar/^{39}Ar$ ages at the base of the core of Chew Bahir should be even older. The sedimentation rate in the lower part of the core would then be even more reduced, which, in addition to the values of the numerical ages, argues against this interpretation. At this point, the identification of further datable material or tephrochronological time markers could help in the future to validate or falsify the models presented here.

All in all, we propose that our combined approach of direct dating and tuning provides a more detailed age model for the Chew Bahir than either the exclusively directly dated age model RRMarch2021 (Roberts et al., 2021) or the exclusively tuned model (Duesing et al., 2021). The new age model RRMarch2021+MHT560 combines the advantages of the directly dated age model RRMarch2021 in the area where many numerical AMS ^{14}C, OSL and $^{40}Ar/^{39}Ar$ dates, as well as the tephrochronological information are available, while the orbitally tuned age model provides arguably better constraint on sediment age for the time interval between 155 and 428 kyr BP, where directly dated material is lacking. Future advances in finding and analyzing datable material in the ~290 m composite Chew Bahir CHB14-2 core may close the gap in the directly dated age model RRMarch2021. Until then, we suggest that based on this combined approach, we can now use the Chew Bahir record for interpretation and correlation on shorter time scales (less than 1–2 precession cycles), which has not been possible so far. This finally facilitates the discussion of temporal differences in climate change as, for example, a driver of cultural innovations or settlement patterns (Grant et al., 2017; Trauth et al., 2019; Schaebitz et al., 2021; Foerster et al., 2022; Trauth et al., 2024).

5. Conclusions

Chew Bahir age models based on direct dating and orbital tuning have been published, but neither provides a convincing model for the entire core. We therefore combined the two approaches to produce a new composite age model RRMarch2021+MHT560. Comparison of the resulting proxy record with ODP Site 967 implies that the composite age model is accurate. The composite age model allows more detailed interrogation of the Chew Bahir record than was previously possible.

CRediT authorship contribution statement

Martin H. Trauth: Writing – review & editing, Writing – original draft, Visualization, Validation, Supervision, Software, Project administration, Methodology, Investigation, Funding acquisition, Formal analysis, Conceptualization. **Asfawossen Asrat:** Conceptualization, Funding acquisition, Investigation, Writing – review & editing. **Markus L. Fischer:** Writing – review & editing, Investigation. **Verena Foerster:** Writing – review & editing, Validation, Investigation, Conceptualization. **Stefanie Kaboth-Bahr:** Conceptualization, Writing – review & editing. **Henry F. Lamb:** Funding acquisition, Investigation, Writing – review & editing. **Norbert Marwan:** Writing – review & editing,

Investigation. **Helen M. Roberts:** Writing – review & editing, Validation, Investigation, Funding acquisition, Conceptualization. **Frank Schaebitz:** Writing – review & editing, Investigation, Funding acquisition.

Declaration of competing interest

The authors declare that they have no known competing financial interests or personal relationships that could have appeared to influence the work reported in this paper.

Data availability

The MATLAB code and data is available online at http://mres.uni-potsdam.de

Acknowledgments

Support for HSPDP has been provided by the International Continental Drilling Program (ICDP). Support has been provided by Germany Research Foundation (DFG) through the Priority Program SPP 1006 ICDP (SCHA 472/13 and/18, TR 419/8,/10 and/16), by the CRC 806 Research Project "Our way to Europe" Project Number 57444011, and by NERC grant NE/K014560/1. The MATLAB code and data is available online at http://mres.uni-potsdam.de. This is publication #56 of the Hominin Sites and Paleolakes Drilling Project.

Appendix A. Supplementary data

Supplementary data to this article can be found online at https://doi.org/10.1016/j.qsa.2024.100208.

References

Amante, C., Eakins, B.W., 2009. ETOPO1 1 Arc-Minute Global Relief Model: Procedures, Data Sources and Analysis. NOAA Technical Memorandum NESDIS NGDC-24. https://doi.org/10.7289/V5C8276M.

Arnold, G.E., Foerster, V., Trauth, M.H., Lamb, H., Schaebitz, F., Asrat, A., Szczech, C., Günter, C., 2021. Advanced hyperspectral analysis of sediment core samples from the Chew Bahir Basin, Ethiopian Rift, in the spectral range from 0.25 to 17 μm: support for climate proxy interpretation. Front. Earth Sci. 9 https://doi.org/10.3389/feart.2021.606588.

Blaauw, M., 2010. Methods and code for classical age-modelling of radiocarbon sequences. Quat. Geochronol. 5, 512–518. https://doi.org/10.1016/j.quageo.2010.01.002.

Blaauw, M., Christen, J.A., 2011. Flexible paleoclimate age-depth models using an autoregressive gamma process. Bayesian Analysis 457–474. https://doi.org/10.1214/11-BA618.

Blaauw, M., Heegard, E., 2012. Estimation of age-depth relationships. In: Birks, et al. (Eds.), Tracking Environmental Change Using Lake Sediments, Developments in Paleoenvironmental Research, vol. 5, pp. 379–413. https://doi.org/10.1007/978-94-007-2745-812.

Bronk Ramsey, C., 2008. Deposition models for chronological records. Quat. Sci. Rev. 27, 42–60. https://doi.org/10.1016/j.quascirev.2007.01.019.

Bronk Ramsey, C., 2017. Methods for summarizing radiocarbon datasets. Radiocarbon 59 (2), 1809–1833. https://doi.org/10.1017/RDC.2017.108.

Channell, J.E.T., Mazaud, A., Sullivan, P., Turner, S., Raymo, M.E., 2002. Geomagnetic excursions and paleointensities in the Matuyama chron at ocean drilling program sites 983 and 984 (Iceland basin). J. Geophys. Res. Solid Earth 107 (11), 1–14. https://doi.org/10.1029/2001JB000491.

Cohen, A., et al., 2016. The Hominin sites and Paleolakes drilling project: inferring the environmental context of human evolution from eastern african rift lake deposits. Sci. Drill. 21, 1–16. https://doi.org/10.1146/annurev-earth-031920-081947.

Cohen, A.S., et al., 2022. Reconstructing the environmental context of human origins in eastern Africa through scientific drilling. Annu. Rev. Earth Planet Sci. 50, 451–476. https://doi.org/10.1146/annurev-earth-031920-081947.

Davidson, A., 1983. The Omo River Project: reconnaissance geology and geochemistry of parts of ilubabor, kefa, gemu gofa and sidamo. Bull. Ethiop. Inst. Geol. Surv. 2, 1–89.

Duesing, W., Berner, N., Deino, A.L., Foerster, V., Kraemer, H., Marwan, N., Trauth, M.H., 2021. Multiband wavelet age modeling (MUBAWA) for a ~293 m (~600 kyr) sediment core from Chew Bahir basin, southern Ethiopian Rift. Front. Earth Sci. 9, 594047 https://doi.org/10.3389/feart.2021.594047.

Fischer, M.L., Munz, P.M., Foerster, V., Schaebitz, F., Marwan, N., Schwanghart, W., Kaboth-Bahr, S., Trauth, M.H., 2024. Spatio-temporal variations of climate along possible African-Arabian routes of H. sapiens expansion. Quat. Sci. Adv. 14, 100174 https://doi.org/10.1016/j.qsa.2024.100174.

Foerster, V., Junginger, A., Langkamp, O., Gebru, T., Asrat, A., Umer, M., Lamb, H., Wennrich, V., Rethemeyer, J., Nowaczyk, N., Trauth, M.H., Schäbitz, F., 2012. Climatic change recorded in the sediments of the Chew Bahir basin, southern Ethiopia, during the last 45,000 years. Quat. Int. 274, 25–37. https://doi.org/10.1016/j.quaint.2012.06.028.

Foerster, V., Asrat, A., Bronk Ramsey, C., Brown, E.T., Chapot, M.S., Deino, A., Deocampo, D.M., Duesing, W., Hahn, A., Junginger, A., Kaboth-Bahr, S., Lane, C.S., Opitz, S., Noren, Roberts, H.M., Stockhecke, M., Tiedemann, R., Vidal, C., Vogelsang, R., Cohen, A.S., Lamb, H.F., Schaebitz, F., Trauth, M.H., 2022. 620,000 years of eastern African climate variability and hominin evolution. Nature Geosci. 15, 805–811. https://doi.org/10.1038/s41561-022-01032-y.

Foerster, V., Deocampo, D., Asrat, A., Günter, C., Junginger, A., Krämer, H., Stroncik, N., Trauth, M.H., 2018. Towards an understanding of climate proxy formation in the Chew Bahir basin, southern Ethiopian Rift. Palaeogeography, Palaeoclimatology, Palaeoecology 501, 111–123. https://doi.org/10.1016/j.palaeo.2018.04.009.

Foerster, V., Junginger, A., Asrat, A., Lamb, H.F., Weber, M., Rethemeyer, J., Frank, U., Brown, M.C., Trauth, M.H., Schaebitz, F., 2014. 46 000 years of alternating wet and dry phases on decadal to orbital timescales in the cradle of modern humans: the Chew Bahir project, southern Ethiopia. Clim. Past Discuss 10, 977–1023. https://doi.org/10.5194/cpd-10-977-2014.

Foerster, V., Vogelsang, R., Junginger, A., Asrat, A., Lamb, H.F., Schaebitz, F., Trauth, M.H., 2015. Environmental change and human occupation of southern Ethiopia and northern Kenya during the last 20,000 years. Quat. Sci. Rev. 129, 333–340. https://doi.org/10.1016/j.quascirev.2015.10.026.

Gebregiorgis, D., Deocampo, D.M., Foerster, V., Longstaffe, F.J., Delaney, J.S., Schaebitz, F., Junginger, A., Markowska, M., Opitz, S., Trauth, M.H., Lamb, H.F., Asrat, A., 2021. Modern sedimentation and authigenic mineral formation in the Chew Bahir basin, southern Ethiopia: implications for interpretation of late quaternary paleoclimate records. Front. Earth Sci. 9, 607695 https://doi.org/10.3389/feart.2021.607695.

Grant, K.M., Rohling, E.J., Westerhold, H., Zabel, M., Heslop, D., Konijnendijk, T., Lourens, L., 2017. A 3 million year index for North African humidity/aridity and the implication of potential pan-African Humid periods. Quat. Sci. Rev. 171, 100–118. https://doi.org/10.1016/j.quascirev.2017.07.005.

Hailemeskel, A., Fekadu, H., 2004. Geological map of Yabello. Addis Ababa ISN 0000 0001 0674 8528. Geological Survey of Ethiopia.

Hassen, N., Yemane, T., Genzebu, W., 1997. Geology of the Agere Maryam Area. Geological Survey of Ethiopia, Addis Ababa.

Hays, J.D., Imbrie, J., Shackleton, N.J., 1976. Variations in the Earth's orbit: pacemaker of the ice ages. Science 194, 1121–1132. http://doi.org/10.1126/science.194.4270.1121.

Key, R.M., 1988. Geology of the Sabarei Area: Degree Sheets 3 and 4, with Coloured 1: 250 000 Geological Map and Results of Geochemical Exploration (Report). Ministry of Environment and Natural Resources. Mines and Geology Dept, Nairobi, Kenya.

Laj, C., Kissel, C., Beer, J., 2013. High resolution global paleointensity stack since 75 kyr (GLOPIS-75) calibrated to absolute values. American Geophysical Union. Timescales Of The Paleomagnetic Field, pp. 255–265. https://doi.org/10.1029/145GM19.

Lowe, D.J., 2011. Tephrochronology and its application: a review. Quat. Geochronol. 6, 107–153. https://doi.org/10.1016/j.quageo.2010.08.003.

Laskar, J., Gastineau, M., Joutel, F., Robutel, P., Levrard, B., Correia, A., 2004. A long term numerical solution for the insolation quantities of Earth. Astron. Astrophys. 428, 261-285. https://doi.org/10.1051/0004-6361:20041335.

Martinson, D.G., Pisias, N.G., Hays, J.D., Imbrie, J., Moore, T.C., Shackleton, N.J., 1987. Age dating and the orbital theory of the ice ages: Development of a high-resolution 0 to 300,000-year chronostratigraphy. Quaternary research 27 (1), 1–29. https://doi.org/10.1016/0033-5894(87)90046-9.

MathWorks, 2023. MATLAB Signal Processing Toolbox – User's Guide. The MathWorks, Inc., Natick, MA.

Meynadier, L., Valet, J.P., Grousset, F.E., 1995. Magnetic properties and origin of upper quaternary sediments in the Somali basin. Indian Ocean Paleoceanogr. 10, 459–472. https://doi.org/10.1029/94PA03151.

Paliwal, K.K., Agarwal, A., Sinha, S.S., 1982. A modification over sakoe and chiba's dynamic time warping algorithm for isolated word recognition. Signal Process. 4, 329–333. https://doi.org/10.1016/0165-1684(82)90009-3.

Pisias, N.G., Martinson, D.G., Moore, Shackleton, N.J., Prell, W., Hays, J., Boden, G., 1984. High resolution stratigraphic correlation of benthic oxygen isotopic records spanning the last 300,000 years. Marine Geology 56 (1–4), 119–136. https://doi.org/10.1016/0025-3227(84)90009-4.

Reimer, P.J., Austin, W., Bard, E., Bayliss, A., Blackwell, P., Bronk Ramsey, C., Butzin, M., Cheng, H., Edwards, R., Friedrich, M., et al., 2020. The IntCal20 northern hemisphere radiocarbon age calibration curve (0–55 cal kBP). Radiocarbon 62 (4), 725–757. https://doi.org/10.1017/RDC.2020.41.

Reimer, P.J., Bard, E., Bayliss, A., Beck, J.W., Blackwell, P.G., Ramsey, C.B., Buck, C.E., Cheng, H., Edwards, R.L., Friedrich, M., Grootes, P.M., Guilderson, T.P., Haflidason, H., Hajdas, I., Hatté, C., Heaton, T.J., Hoffmann, D.L., Hogg, A.G., Hughen, K.A., Kaiser, K.F., Kromer, B., Manning, S.W., Niu, M., Reimer, R.W., Richards, D.A., Scott, E.M., Southon, J.R., Staff, R.A., Turney, C.S.M., Plicht, J. van der, 2013. IntCal13 and Marine13 radiocarbon age calibration curves 0–50,000 years cal BP. Radiocarbon 55, 1869-1887. https://doi.org/10.2458/azu_js_rc.55.16947.

Roberts, H.M., Bronk Ramsey, C., Chapot, M.S., Deino, A.L., Lane, C.S., Vidal, C., Asrat, A., Cohen, A., Foerster, V., Lamb, H.F., Schäbitz, F., Trauth, M.H., Viehberg, F. A., 2021. Using multiple chronometers to establish a long, directly-dated lacustrine record: constraining >600,000 years of environmental change at Chew Bahir, Ethiopia. Quat. Sci. Rev. 266, 107025 https://doi.org/10.1016/j.quascirev.2021.107025.

Sakoe, H., Chiba, S., 1978. Dynamic programming algorithm optimization for spoken word recognition. IEEE Trans. Acoust. Speech Signal Process. 26, 43–49. https://doi.org/10.1109/TASSP.1978.1163055.

Schaebitz, F., et al., 2021. Hydroclimate changes in eastern Africa over the past 200,000 years may have influenced early human dispersal. Nat. Commun. Earth Environ. 2, 123. https://doi.org/10.1038/s43247-021-00195-7.

Singer, B.S., Relle, M.R., Hoffman, K.A., Battle, A., Guillou, H., Laj, C., Carracedo, J.C., 2002. Ar/Ar ages of transitionally magnetized lavas on La Palma, Canary Islands, and the geomagnetic instability timescale. J. Geophys. Res. 107 (B11), 2307. https://doi.org/10.1029/2001JB001613.

Trauth, M.H., 2014. A new probabilistic technique to build an age model for complex stratigraphic sequences. Quat. Geochronol. 22, 65–71. https://doi.org/10.1016/j.quageo.2014.03.001.

Trauth, M.H., Bergner, A.G.N., Foerster, V., Junginger, A., Maslin, M.A., Schaebitz, F., 2015. Episodes of environmental stability and instability in late cenozoic lake records of eastern Africa. J. Hum. Evol. 87, 21–31. https://doi.org/10.1016/j.jhevol.2015.03.011.

Trauth, M.H., Foerster, V., Junginger, A., Asrat, A., Lamb, H., Schaebitz, F., 2018. Abrupt or gradual? Change point analysis of the late pleistocene-holocene climate record from Chew Bahir, southern Ethiopia. Quat. Res. 90, 321–330. https://doi.org/10.1017/qua.2018.30.

Trauth, M.H., Asrat, A., Duesing, W., Foerster, V., Kraemer, K.H., Marwan, N., Maslin, M.A., Schaebitz, F., 2019. Classifying past climate change in the Chew Bahir basin, southern Ethiopia, using recurrence quantification analysis. Clim. Dynam. 53, 2557–2572. https://doi.org/10.1007/s00382-019-04641-3.

Trauth, M.H., Asrat, A., Cohen, A., Duesing, W., Foerster, V., Kaboth-Bahr, S., Kraemer, H., Lamb, H., Marwan, N., Maslin, M., Schaebitz, F., 2021. Recurring types of variability and transitions in the ~620 kyr record of climate change from the Chew Bahir basin, southern Ethiopia. Quat. Sci. Rev. 266, 106777 https://doi.org/10.1016/j.quascirev.2020.106777.

Trauth, M.H., Asrat, A., Fischer, M.L., Hopcroft, P.O., Foerster, V., Kaboth-Bahr, S., Kindermann, K., Lamb, H.F., Marwan, N., Maslin, M.A., Schaebitz, F., Valdes, P.J., 2024. Early Warning Signals of the Termination of the African Humid Period(s). Nat. Commun. 15, 3697. https://doi.org/10.1038/s41467-024-47921-1.

Vidal, C.M., Fontijn, K., Lane, C.S., Asrat, A., Barfod, D., Tomlinson, E.L., Piermattei, A., Hutchison, W., Tadesse, A.Z., Yirgu, G., Deino, A., Moussallam, Y., Mohr, P., Williams, F., Mather, T.A., Pyle, D.M., Oppenheimer, C., 2022. Geochronology and glass geochemistry of major pleistocene eruptions in the Main Ethiopian Rift: Towards a regional tephrostratigraphy. Quat. Sci. Rev. 290, 107601 https://doi.org/10.1016/j.quascirev.2022.107601.

Viehberg, F.A., Just, J., Dean, J.R., Wagner, B., Franz, S.O., Klasen, N., Kleinen, T., Ludwig, P., Asrat, A., Lamb, H.F., Leng, M.J., Rethemeyer, J., Milodowski, A.E., Claussen, M., Schäbitz, F., 2018. Environmental change during MIS4 and MIS 3 opened corridors in the Horn of Africa for Homo sapiens expansion. Quat. Sci. Rev. 202, 139–153. https://doi.org/10.1016/j.quascirev.2018.09.008.

Wessel, P., Smith, W.H.F., 1996. A Global Self-consistent, Hierarchical, High-resolution Shoreline Database. J. Geophys. Res. 101 (B4), 8741–8743. https://doi.org/10.1029/96JB00104.